Smart Structures Systems, *Vol. 20, No. 6 (2017) 729-737*
DOI: https://doi.org/10.12989/sss.2017.20.6.729

Linear shell elements for active piezoelectric laminates

Gil Rama[*1], Dragan Z. Marinkovic[1,2a] and Manfred W. Zehn[1b]

[1]*Department of Structural Analysis, Berlin Institute of Technology, Germany*
[2]*Faculty of Mechanical Engineering, University of Nis, Serbia*

(Received July 1 2017, Revised October 24, 2017, Accepted October 25, 2017)

Abstract. Piezoelectric composite laminates are a powerful material system that offers vast options to improve structural behavior. Successful design of piezoelectric adaptive structures and testing of control laws call for highly accurate, reliable and numerically efficient numerical tools. This paper puts focus onto linear and geometrically nonlinear static and dynamic analysis of smart structures made of such a material system. For this purpose, highly efficient linear 3-node and 4-node finite shell elements are proposed. Both elements employ the Mindlin-Reissner kinematics. The shear locking effect is treated by the discrete shear gap (DSG) technique with the 3-node element and by the assumed natural strain (ANS) approach with the 4-node element. Geometrically nonlinear effects are considered using the co-rotational approach. Static and dynamic examples involving actuator and sensor function of piezoelectric layers are considered.

Keywords: active structure; linear shell element; piezoelectricity; co-rotational FEM; geometric nonlinearity

1. Introduction

More than two decades ago the idea of adaptive/smart structures has seen the light of day. It denoted the conceptual change of structures from passive, deformable systems to active systems capable of sensing changes in their condition and performing adequate actions to resist undesired changes (Gabbert and Tzou 2000). The idea has opened up vast possibilities to improve structural behavior and features such as vibration suppression (Li and Yao 2016, Oveisi and Nestorovic 2016), noise attenuation (Aridogan and Basdogan 2015, Gabbert *et al*. 2017), shape control (Zhang *et al*. 2016, Zhang *et al*. 2017), energy harvesting (Biswal *et al*. 2017, Aladwani *et al*. 2014), structural health monitoring (Masmoudi *et al*. 2015, Vertuccio *et al*. 2016), quantitative damage identification (Huynh and Kim 2017), thus offering improved safety, robustness and comfort.

Shell structures with piezoelectric active elements, as a distinctive group of adaptive structures, have drawn a great deal of attention from the research community. This may be attributed to the fact that the majority of engineering structures are thin-walled structures. Additionally, by adding/embedding active elements in the form of thin piezoelectric patches, the thin-walled structures can be converted into adaptive systems in a relatively simple manner. Piezoelectric material based active elements are a common choice for this purpose, as they operate in the required frequency range and offer adequate force, electric voltage and stroke ranges for this type of structures. The piezoelectric patches are used as both actuators (reverse piezoelectric effect) and sensors (direct piezoelectric effect).

Design of such structures calls for accurate, reliable and efficient numerical tools. This enables optimization in the early design stages related to the structure's geometry, size, number and position of active elements as well as different parameters of the control algorithms. The finite element method (FEM) is typically addressed as the most powerful tool in the field of structural analysis. A number of researchers dedicated their work to the development of various finite elements for modeling and simulation of piezoelectric active structures.

Three-dimensional solid elements do not represent the first choice when global structural behavior of thin-walled structures is aimed at. However, they offer insight into some local effects not covered by typical shell elements and were therefore addressed in the work of some researchers. They require additional techniques to improve their performance when used for modeling shell type of structures. Lee *et al*. (2004) developed an 18-node solid element with the assumed strain technique. Braess and Kaltenbacher (2008) used balanced reduced integration in the thickness direction, applied only to a portion of the shear term, to formulate a quadratic hexahedral piezoelectric element. Willberg and Gabbert (2012) based a 3D piezoelectric finite element for smart structures on the isogeometric approach.

A number of researchers aimed at formulations that are essentially two-dimensional but offer accuracy and fidelity close to three-dimensional formulations. Those efforts resulted in layerwise theories. The Carrera Unified Formulation (CUF) (Carrera 2003) was used in a number of element formulations (Cinefra *et al.* 2015a, b). The formulation was also used by Valvano and Carrera (2017) to develop variable kinematic shell elements, in which both the equivalent single layer approach and the layerwise approach are used together to combine their advantages in the case of purely mechanical field. This formulation was extended by Carrera and Valvano (2017) to

*Corresponding author, Ph.D. student
E-mail: gil.rama@tu-berlin.de
[a] Ph.D.
[b] Professor

ISSN: 1738-1584 (Print), 1738-1991 (Online)

coupled electro-mechanical problems.

In most developments of piezoelectric shell elements, equivalent single layer based theories were addressed as they offer a very good balance between the accuracy and numerical effort when the global structural behavior is aimed at. The body of literature on the topic is prohibitively large for an exhaustive overview. Both the classical laminate theory (Kirchhoff-Love kinematical assumptions) and the First Order Shear Deformation theory (Mindlin-Reissner kinematical assumptions) were used in the developments, the latter being more often addressed. The developed elements include both numerically highly efficient linear shell elements (To and Liu 2003, Zemčík *et al*. 2007) and curved quadratic shell elements (Gabbert *et al*. 2002, Marinkovic *et al*. 2006) with various techniques implemented to alleviate the locking phenomena. Although most of the developments are for linear analysis, some of the researchers also tackled the problems of geometrically nonlinear analysis in their work (Simoes Moita *et al*. 2002, Rabinovitch 2005, Lentzen *et al*. 2007, Marinkovic *et al*. 2008, Rama 2017). Some of the developed elements were also implemented in commercial software packages by means of user subroutines (Nestorovic *et al*. 2013, Nestorovic *et al*. 2014), while a number of studies were aimed at different aspects in modeling piezoelectric coupled-field effects (Marinkovic *et al*. 2009, Piefort 2002, Marinkovic and Marinkovic 2012, Zhang 2014).

In this paper, two numerically highly efficient, linear shell elements are presented for modeling piezoelectric shell structures with piezopatches polarized in the thickness direction. The formulation of the triangular and quadrilateral elements is extended to geometrically nonlinear analysis. For this purpose a co-rotational approach (Felippa and Haugen 2005, Nguyen *et al*. 2016) is used.

2. Geometry and mechanical field of the elements

For the sake of brevity, in further text the linear triangular and quadrilateral shell elements will be referred to as SH3 and SH4ANS, respectively.

For treatment of the transverse shear locking effect, the SH3 element uses the discrete shear gap technique as proposed by Bletzinger *et al*. (2000) while the SH4ANS element relies on the assumed natural strain (ANS) approach. In addition, to improve the accuracy and stability of the SH3 element, the cell strain smoothing technique proposed by Nguyen-Thoi *et al*. (2013) is implemented.

Beside the global coordinate system, (x, y, z), the formulation of both elements requires also a local coordinate system, (x′, y′, z′), Fig. 1. It is defined so that the local x′-axis is oriented from element node 1 towards node 2, while the z′-axis is perpendicular to the plane defined by the x′-axis and a vector orientated from node 1 to node 3. The local y′-axis is then easily obtained by the cross-product.

The shell geometry with respect to the local coordinate system is practically regenerated from its mid-surface

$$\begin{Bmatrix} x' \\ y' \\ z' \end{Bmatrix} = \sum_{i=1}^{n} N_i \begin{Bmatrix} x'_i \\ y'_i \\ 0 \end{Bmatrix} + \sum_{i=1}^{n} \frac{h}{2} N_i t \{ e_{z'} \} \tag{1}$$

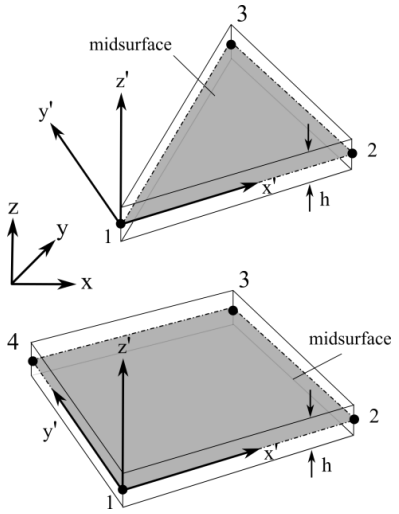

Fig. 1 Geometry and the local coordinate systems of the 3-node and 4-node shell elements

where h is the shell thickness, N_i are the shape functions, n indicates the number of nodes of the element (for SH3 n = 3; for SH4ANS n = 4), $\{e_{z'}\}$ is the unit vector of the z′-axis, and -1 < t < +1. The elements are based on the Mindlin-Reissner kinematical assumption and, hence, the displacement field is given in terms of the mid-surface displacements u', v' and w' along the local x′, y′ and z′ axes, respectively, and the rotations $\theta_{ix'}$ and $\theta_{iy'}$ around the local x′ and y′ axes

$$\begin{Bmatrix} u' \\ v' \\ w' \end{Bmatrix} = \sum_{i=1}^{n} N_i \begin{Bmatrix} u'_i \\ v'_i \\ w'_i \end{Bmatrix} + \sum_{i=1}^{n} \frac{h}{2} N_i t \begin{Bmatrix} \theta_{iy'} \\ -\theta_{ix'} \\ 0 \end{Bmatrix} \tag{2}$$

The strain field with respect to the local element coordinate system can be represented in the following form

$$\{\varepsilon'\} = \begin{Bmatrix} \{\varepsilon'_{mf}\} \\ -- \\ \{\varepsilon'_s\} \end{Bmatrix} = \begin{bmatrix} [B_m] + z'[B_b] \\ -- \\ [B_s] \end{bmatrix} \{d'\} = [B_u]\{d'\} \tag{3}$$

with the membrane-flexural (in-plane) strain field $\{\varepsilon'_{mf}\}$, the transverse shear strains $\{\varepsilon'_s\}$, the strain-displacement matrices for the membrane $[B_m]$, bending $[B_b]$ and transverse shear part $[B_s]$ and the nodal degrees of freedom vector $\{d'\}$.

The nodal membrane-flexural strain displacement matrices are given in the same way for both element formulations

$$[B_{m,i}] = \begin{bmatrix} N_{i,x'} & 0 & 0 & 0 & 0 \\ 0 & N_{i,y'} & 0 & 0 & 0 \\ N_{i,y'} & N_{i,x'} & 0 & 0 & 0 \end{bmatrix} \tag{4}$$

$$[B_{b,i}] = \begin{bmatrix} 0 & 0 & 0 & 0 & N_{i,x'} \\ 0 & 0 & 0 & -N_{i,y'} & 0 \\ 0 & 0 & 0 & -N_{i,x'} & N_{i,y'} \end{bmatrix} \tag{5}$$

where $N_{i,x'}$ and $N_{i,y'}$ are the derivatives of the corresponding

shape functions with respect to the local axes x′ and y′.

The treatment of the transverse strain field differs between the two elements. The triangular element uses the discrete shear gap approach (DSG) which separates the transverse deflections in parts due to pure bending and due to shear. The resulting strain-displacement matrices for the shear strain are given in the closed form as follows (Bletzinger *et al*. 2000)

$$\begin{aligned}
[B_{s,1}] &= \frac{1}{2A_e}\begin{bmatrix} 0 & 0 & b-c & 0 & A_e \\ 0 & 0 & d-a & -A_e & 0 \end{bmatrix} \\
[B_{s,2}] &= \frac{1}{2A_e}\begin{bmatrix} 0 & 0 & c & -bc/2 & ac/2 \\ 0 & 0 & -d & bd/2 & -ad/2 \end{bmatrix} \\
[B_{s,3}] &= \frac{1}{2A_e}\begin{bmatrix} 0 & 0 & -b & bc/2 & -bd/2 \\ 0 & 0 & a & -ac/2 & ad/2 \end{bmatrix}
\end{aligned} \tag{6}$$

with the parameters *a*, *b*, *c* and *d* given by

$$\begin{aligned}
a &= x'_2 - x'_1 \quad b = y'_2 - y'_1 \\
c &= y'_3 - y'_1 \quad d = x'_3 - x'_1
\end{aligned} \tag{7}$$

The shear strain field of the four node element is replaced by the assumed natural strain (ANS) field (Militello and Felippa 1990) which is interpolated by conforming strains at four tying points A, B, C and D depicted in Fig. 2, so that

$$\{\varepsilon'_s\} = \begin{Bmatrix} \frac{1}{2}(1-\xi)\gamma^{A}_{y'z'} + \frac{1}{2}(1+\xi)\gamma^{C}_{y'z'} \\ \frac{1}{2}(1-\eta)\gamma^{B}_{x'z'} + \frac{1}{2}(1+\eta)\gamma^{D}_{x'z'} \end{Bmatrix} = \begin{bmatrix} B^{y'z'}_{s,ANS} \\ B^{x'z'}_{s,ANS} \end{bmatrix}\{d'\} \tag{8}$$

where $\gamma_{x'z'}$ and $\gamma_{y'z'}$ are the transverse shear strains in the x′z′ and y′z′ planes.

The 3-node element is further improved by applying the strain smoothing technique (Nguyen-Thoi *et al*. 2013), which implies division of the element into three sub-triangles using the element centroid as an additional node. The strain-displacements matrices are computed for each sub-triangle and then averaged, whereby the assumption is implemented that the displacement of the centroid is given as an average of the displacements at nodes.

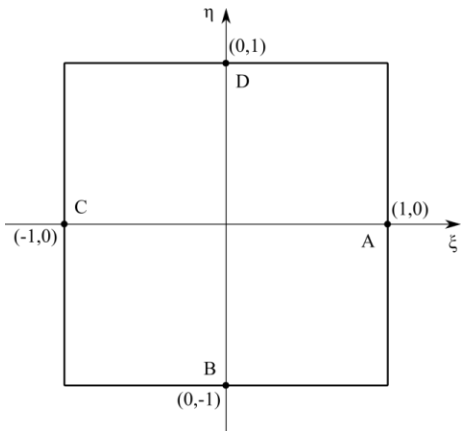

Fig. 2 Position of the tying points for the assumed strains

Finally, the element mechanical stiffness matrix in the local coordinate system is for both elements given by

$$[K_e] = \int_{V_e} \left([B_u]^T [C][B_u] \right) dV_e \tag{9}$$

with [*C*] denoting the Hooke's matrix. Integration in the thickness direction is performed analytically. In the case of laminates involving orthotropic fiber-reinforced composite layers this results in the well-known ABD (membrane-flexural part) and F (transverse shear part) matrices (Berthelot 1999), while the integration over the surface is performed numerically:

$$\begin{aligned}
[K_e] = &\int_{A_e} \left(\begin{bmatrix} [B_m] & [0] \\ [0] & [B_b] \end{bmatrix}^T \begin{bmatrix} [A] & [B] \\ [B] & [D] \end{bmatrix} \begin{bmatrix} [B_m] & [0] \\ [0] & [B_b] \end{bmatrix} \right) dA_e \\
&+ \int_{A_e} [B_s]^T [F][B_s] dA_e
\end{aligned} \tag{10}$$

With the SH4ANS element, the full integration scheme is used. Since the strain-displacement matrices of the SH3 element are constant over the element domain, the integration comes down to multiplication with the element area A_e.

3. The piezoelectric coupling and the electric field

Piezoelectric materials generate an electric field when subjected to mechanical deformation (direct piezoelectric effect) and strain when electric voltage is applied (reverse piezoelectric effect). The linear piezoelectric constitutive equations read

$$\begin{aligned}
\{\sigma\} &= [C^E]\{\varepsilon\} - [e]\{E\} \\
\{D\} &= [e]\{\varepsilon\} + [d^\varepsilon]\{E\}
\end{aligned} \tag{11}$$

with $\{\sigma\}$ denoting the mechanical stress (Voigt notation), $[C^E]$ the piezoelectric material Hooke's matrix at constant electric field $\{E\}$, $\{D\}$ is the electric displacement vector, $[d^\varepsilon]$ is the dielectric permittivity matrix at constant strain $\{\varepsilon\}$, and $[e]$ denotes the piezoelectric coupling matrix.

In the present formulation the piezoelectric patches are assumed to be polarized in the thickness direction and operating on the e_{31}-effect, which couples the electric field in the thickness direction, *E*, with the in-plane strains. Typical approximation yielding constant electric field over the thickness of the piezopatch is applied, yielding for the k^{th} piezolayer

$$E_k = -\frac{\Delta\Phi_k}{h_k} \tag{12}$$

where $\Delta\Phi_k$ is the difference of electric potentials of the k^{th} piezolayer with the thickness h_k. Hence, the electric field – electric potential matrix, $[B_\phi]$, is diagonal with $1/h_k$ as a typical element on the main diagonal. Hence, the element piezoelectric coupling and dielectric stiffness matrices read, respectively

$$\left[K_{u\phi,e}\right]=\int_V\left(\begin{bmatrix}[B_m]\\ z'[B_b]\end{bmatrix}^T[e][B_\phi]\right)dV \tag{13}$$

$$\left[K_{\phi\phi,e}\right]=-\int_V[B_\phi]^T\left[d^{\varepsilon}\right][B_\phi]dV \tag{14}$$

4. Finite element equations and the co-rotational approach

The FE equations for the piezoelectric continuum are given below for the most general case considered here - geometrically nonlinear dynamic case

$$\begin{aligned}&\begin{bmatrix}[M_{uu}] & [0]\\ [0] & [0]\end{bmatrix}\begin{Bmatrix}{}^{t+\Delta t}\{\ddot{u}\}^{(k)}\\ \{0\}\end{Bmatrix}\\&+\begin{bmatrix}{}^{t+\Delta t}[C_{uu}] & [0]\\ [0] & [0]\end{bmatrix}\begin{Bmatrix}{}^{t+\Delta t}\{\dot{u}\}\\ \{0\}\end{Bmatrix}\\&+\begin{bmatrix}{}^{t}[K_{uuT}] & {}^{t}[K_{u\phi}]\\ {}^{t}[K_{\phi u}] & {}^{t}[K_{\phi\phi}]\end{bmatrix}\begin{Bmatrix}{}^{t}\{\Delta u\}^{(k)}\\ {}^{t}\{\Delta\phi\}^{(k)}\end{Bmatrix}\\&=\begin{Bmatrix}{}^{t+\Delta t}\{F_{ext}\}-{}^{t+\Delta t}\{F_{in}\}^{(k-1)}\\ {}^{t+\Delta t}\{Q_{ext}\}-{}^{t+\Delta t}\{Q_{in}\}^{(k-1)}\end{Bmatrix}\end{aligned} \tag{15}$$

with $[M_{uu}]$ denoting the global mass matrix, $[C_{uu}]$ is the mechanical damping matrix, $[K_{uuT}]$, $[K_{u\phi}]$, $[K_{\phi u}]$, $[K_{\phi\phi}]$ and $[K_\sigma]$ are the tangent global mechanical stiffness, piezoelectric direct and inverse coupling, the dielectric stiffness matrices, respectively The vectors $\{\Delta\phi\}$, $\{\Delta u\}$, $\{\dot{u}\}$, $\{\ddot{u}\}$ are the incremental differences of electric potentials of the piezolayers, incremental displacements, nodal velocities and accelerations, respectively. On the right hand-side of the FE equations are the external and internal mechanical forces, $\{F_{ext}\}$ and $\{F_{in}\}$, as well as the external and internal electric charges, $\{Q_{ext}\}$ and $\{Q_{in}\}$. The left superscript denotes the time, and since the solution proceeds iteratively, the index (k) in the right superscript is the iteration number. The FE equations for the static case are obtained by neglecting the inertia and damping effects in the mechanical field, while in the linear case the total displacements and electric potentials are used on the left-hand side of the equations, and, on the right hand-side, the internal forces and electric charges are removed (they are given on the left-hand side by the product of the linearized generalized stiffness matrix and total displacements and electric potentials).

In order to cover the geometrically nonlinear effects in an efficient manner, the co-rotational approach is used. It is used in a simplified form (Marinkovic *et al*. 2012) which implies that the element motion is decomposed into a rigid-body motion, described by the rotation matrix, $[R_e]$, and deformable motion. As a consequence, the linear part of the element stiffness matrix is updated in a straight-forward manner

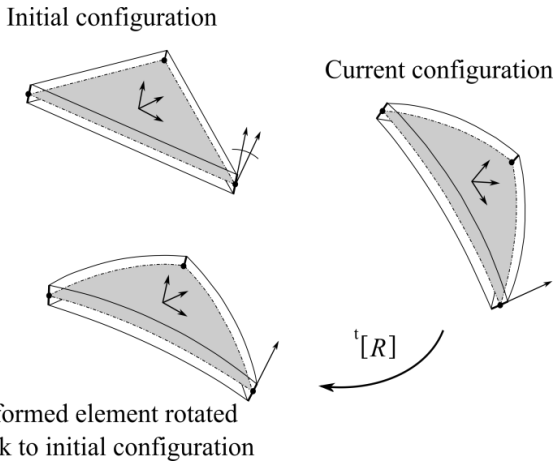

Fig. 3 Co-rotational approach

$${}^{t}\left[K_e^R\right]={}^{t}[R_e]^{0}[K_e]{}^{t}[R_e]^T \tag{16}$$

The element rigid-body rotation is obtained by the polar decomposition of the element deformation gradient. It is constant for the whole domain of the SH3 element. In the case of SH4ANS element, the deformation gradient at the element centroid is used.

The internal forces are determined using the rotation-free displacements, obtained by rotating the current configuration backwards, i.e., through $[R_e]^T$, and comparing the obtained configuration with the initial one. A similar procedure is used to obtain the internal moments, with the remark that the nodal normals are updated using nodal rotations and then rotated back from the current to initial configuration using $[R_e]^T$ in order to get the deformational rotations. The essence of the approach is illustrated in Fig. 3. More details on this procedure can be found in (Marinkovic and Rama 2017).

The geometric stiffness matrix is added to the rotated element linear stiffness matrix in order to obtain the tangent mechanical stiffness matrix. The geometric stiffness matrix is obtained as follows

$$\left[K_{\sigma,e}\right]=\int_{V_e}[G]^T[S][G]dV_e \tag{17}$$

where $[S]$ is the stress matrix comprising the in-plane stress components, while $[G]$ includes the partial derivatives of the shape functions (Crisfield 1991). Finally, the element mechanical tangent stiffness matrix is simply the sum of the rotated linear stiffness matrix and the geometric stiffness matrix

$$\left[K_{uuT,e}\right]=\left[K_e^R\right]+\left[K_{\sigma,e}\right] \tag{18}$$

5. Numerical examples

In the following, a set of examples is studied in order to demonstrate the applicability of the presented elements in linear and geometrically nonlinear static and dynamic

analysis of smart thin-walled structures. Both sensor and actuator function of piezoelectric layers will be considered. The below considered structures are made of composites with various combinations of fiber-reinforced, isotropic and piezoelectric layers. The materials properties, thickness and stacking sequence of the layers vary in the examples and will be specified for each example separately where Y denotes the Young's modulus and ν the Poisson's ratio (with indices referring to the material orientation, where applicable).

5.1 Clamped active beam

In the first example the deflection of a clamped beam under piezoactuation is computed and compared with the experimental results obtained by Gupta *et al*. (2004). The beam geometry and the position of a pair of piezopatches are depicted in Fig. 4. The two oppositely polarized piezopatches made of PSI-5A-S4-ENH are bonded onto the upper and lower surface (Fig. 4) of the host structure made of aluminum. Material properties of both passive and active materials are given in Table 1.

The same voltage of 90 V is supplied to both piezopatches. As the patches are restrained (glued onto the surface), compressive or tensile stresses are induced depending on their polarizations. Hence, the actuation gives rise to the bending moments uniformly distributed along the edges of the surface covered by the piezopatches. The resulting vertical displacements along the beam centerline are computed using the presented elements. Upon convergence analysis, the results obtained with 400 SH3 elements and 200 SH4ANS elements are taken as representative. The computed deflection is depicted in Fig. 5 and it is obviously in a very good agreement with the experimental data by Gupta *et al*. (2004). The results by the SH3 and the SH4ANS elements are almost congruent.

5.2 Simply supported active composite plate

In the following example a simply supported laminated composite plate (0.2 m × 0.2 m) with two oppositely polarized piezoelectric ceramic layers is studied. The plate consists of four graphite–epoxy (T300/976) composite layers, each 0.25 mm thick, and the two piezolayers (PZTG1195N), each 0.1 mm thick. The laminate stacking sequence reads $[p/-45/45]_S$. The geometry is depicted in Fig. 6 and the material properties are summarized in Table 2.

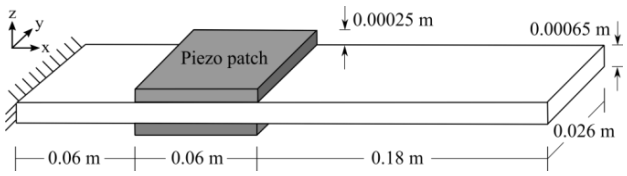

Fig. 4 Geometry of the clamped active beam

Table 1 Clamped active beam - material properties

	Aluminuim	PSI-5A-S4-ENH
Elastic properties		
Y [MPa]	63.8	47.6
ν [-]	0.29	0.3
Piezoelectric constants		
$e_{31} = e_{32}$ [Cm^{-2}]		17.91

Table 2 Active composite plate - material properties

	T300/976	PTZ-G1195
Elastic properties		
Y_{11} [GPa]	150.0	63.0
Y_{22} [GPa]	9.0	63.0
Y_{33} [GPa]	9.0	63.0
υ_{12} [-]	0.3	0.3
υ_{13} [-]	0.3	0.3
υ_{23} [-]	0.3	0.3
Piezoelectric properties		
$e_{31} = e_{32}$ [Cm^{-2}]		22.86
d_{31} (× 10^{-8}) [F/m]		0.0254

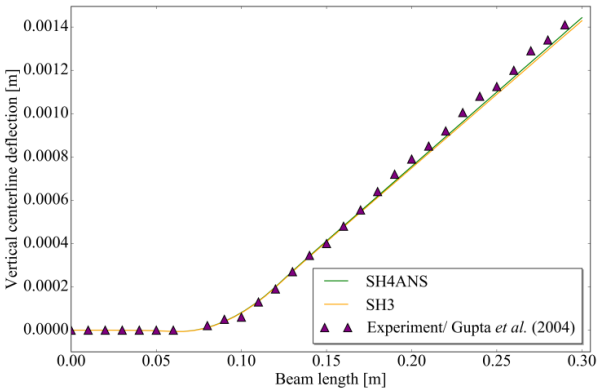

Fig. 5 Vertical displacements along the beam centerline

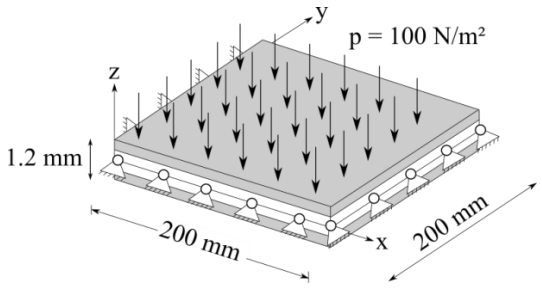

Fig. 6 Geometry of simply supported piezoelectric composite plate

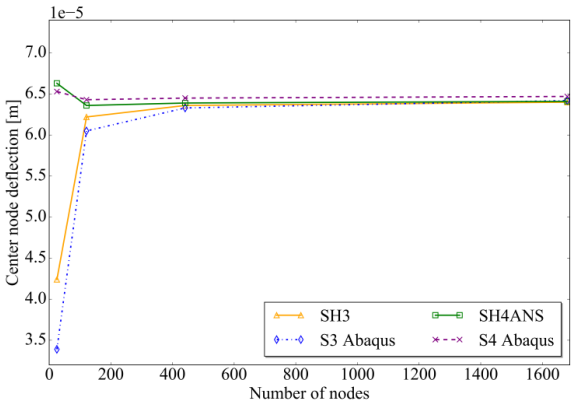

Fig. 7 Active plate - convergence of the FE results

Table 3 Active plate mid-point deflection

Center node displacement $\|w\|\ 10^{-5}$ [m]			
Input voltage [V]	0 V	5 V	10 V
SH3	6.36	2.80	-0.76
SH4ANS	6.39	2.83	-0.73
Liu *et al*. (2004)	6.04	2.72	-0.60

First, the plate is exposed to a uniformly distributed pressure load of 100 N/m^2 and a static analysis is performed. The convergence analysis of the FE results is studied using the presented elements and the Abaqus S3 and S4 shell elements. The deflection of the plate mid-point is observed as a representative result. The diagram in Fig. 7 shows that the results by each of the SH3 and SH4ANS elements exhibit similar convergence rate and behavior as the results by their Abaqus counterparts.

In the further analyses, for each element the corresponding mesh consisting of 441 nodes is used. It is obvious from Fig. 7 that all the considered elements yield a reasonably good result with such a mesh (the results by all four elements with the corresponding meshes containing 441 nodes differ by less than 1%). Liu *et al*. (2004) computed this case using a radial point interpolation method, which belongs to the group of meshless methods, and obtained the plate mid-point deflection of $6.038 \cdot 10^{-5}$ m using 225 nodes. This result differs from the FE results reported here by 5.7 %.

In the next step actuator input voltages of 0V, 5V and 10V are applied across the thickness of the two piezolayers. Similarly to the previous case, the outcome of the actuation is a uniformly distributed bending moments, which in this case acts along the edges of the plate. Table 3 gives the results by the SH3 and SH4ANS elements together with those reported by Liu *et al* (2004).

Furthermore a dynamic analysis is performed in which the piezolayers are considered to operate as sensors. The plate is subjected to a time dependant (harmonic) uniform pressure with an amplitude of 400 Nm^{-2} and a frequency of 200 Hz. The analysis is performed as linear and geometrically nonlinear and the deflection of the plate mid-point is depicted in Fig. 8 and Fig. 9, respectively. In the analysis a constant time-step of 0.00005 s was used. One may notice a good agreement of the results obtained by the presented and Abaqus shell elements.

The sensor voltage responses of the upper (1) and lower (2) piezoelectric layers are more interesting. The linear analysis neglects the change in the structural configuration and, hence, the deformation is bending dominated (the transverse shear effects are present but without influence on the sensor voltage). The piezolayers are oppositely polarized and since they have symmetric position with respect to the neutral plane (while one layer is in tension, the other is in compression), they yield the same sensor voltage, Fig. 10. On the other hand, the geometrically nonlinear analysis accounts for the change in structural configuration. During the deformation the plate becomes essentially a shell and the membrane effects are also present. The sensor voltages reflect the averaged in-plane strains in the piezolayers and the strains are due to both bending and membrane effects. Consequently, the resulting sensor voltages of the two layers differ, Fig. 10. This case emphasizes the need to account for the geometrically nonlinear effects in the behavior of the considered structures. Whereas the deflections do not stress out this need, the fact that the sensor voltages of the two piezolayers exhibit obvious differences does. Their accurate prediction is namely essential for the control algorithms.

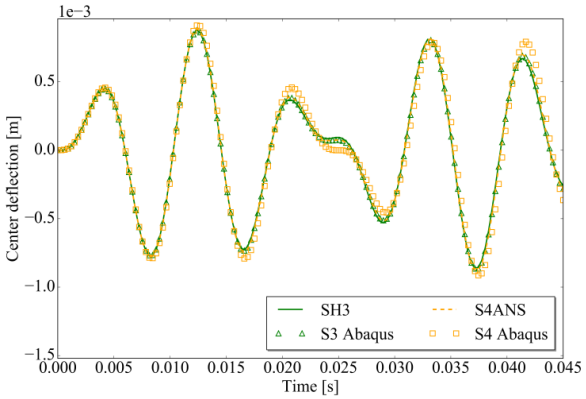

Fig. 8 Linear dynamic analysis – mid-point deflection

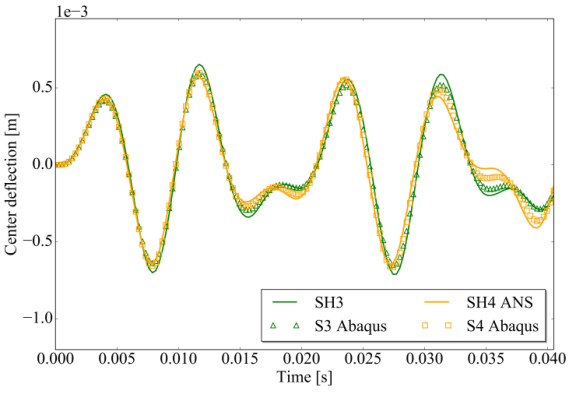

Fig. 9 Geometrically nonlinear dynamic analysis – mid-point deflection

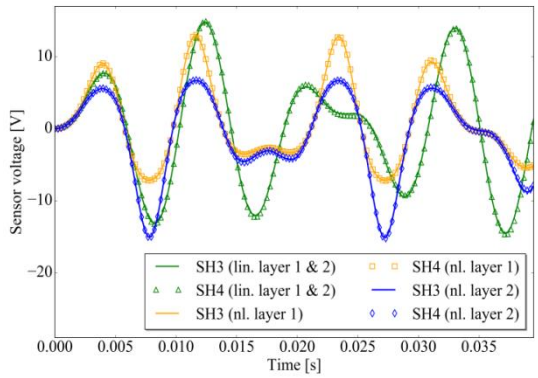

Fig. 10 Linear and geometrically nonlinear dynamic analysis – sensor voltages

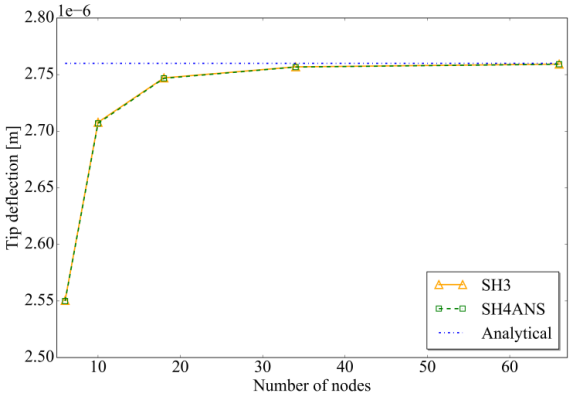

Fig. 12 Curved bimorph beam - convergence of the FE results

5.3 Curved bimorph beam

A simply curved structure (with constant radius of curvature and about only one axis) is considered next. The curved bimorph beam depicted in Fig. 11 consists of two piezoelectric layers with opposite polarization. The radius R of the quarter-ring cantilever beam is 0.2 m and the thickness h is 0.001 m.

A unit voltage Φ = 1 V is applied across the beam thickness, thus causing bending of the structure. The Young's modulus Y is 2 GPa and the piezoelectric constant e is 0.046 Cm^{-2}. The Poisson's ratio is set equal to zero for the sake of comparison with the analytical solution obtained by means of the Castigliano's theorem (Zemčík *et al*. 2007), which yields the following transverse deflection of the beam tip

$$w = 3\frac{e\Phi r^2}{Yh^2} = 2.76\cdot 10^{-6}\,\text{m} \tag{19}$$

The FE results are obtained using different meshes (6, 10, 18, 34 and 66 nodes) and the convergence of the obtained results for the tip deflection is observed. The results for the presented elements are given in the diagram in Fig. 12. It may be noticed that the results by the SH3 and SH4ANS elements converge relatively fast toward the analytical solution and exhibit practically identical convergence rate in this case, when the number of nodes in the FE mesh is used as a parameter of the mesh density.

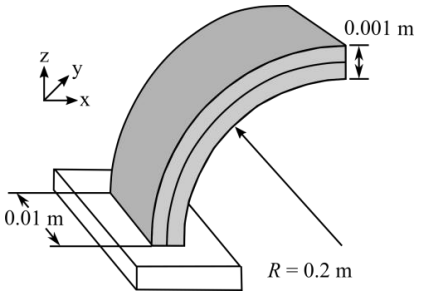

Fig. 11 Geometry of the curved bimorph beam

5.4 Active funnel shaped structure

Finally, the performance of the presented shell elements in modeling arbitrarily curved thin-walled structures is studied. For this purpose, a double curved funnel shaped structure under piezoactuation is considered. The example was originally proposed by Nestorovic *et al*. (2014).

The 0.5 mm thick funnel shaped host structure is made of aluminum and its top and bottom surface are completely covered by piezoelectric layers with a thickness of 0.2 mm. The material properties are given in Table 4 and the geometry is depicted Fig. 13. The structure is considered to be clamped along its lower base, Fig. 13, left.

The actuation is achieved by supplying the oppositely polarized piezolayers with the electric voltage of 100 V. The symmetry of geometry, boundary conditions and excitation allows to model only one quarter of the structure with the additional symmetric boundary conditions applied.

In the first step a convergence study is carried out in order to evaluate the convergence rate of the presented shell elements in modeling double curved structures. The displacement magnitude (U_{sum}) at point A, Fig. 13, is observed as a representative result.

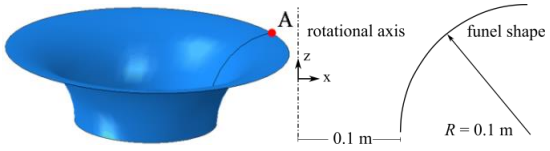

Fig. 13 Geometry of the funnel shaped structure

Table 4 Funnel shaped structure material properties

	Aluminuim	Piezomaterial
Elastic properties		
Y [Mpa]	70.3	60.0
v [-]	0.34	0.3
Piezoelectric constants		
$e_{31} = e_{32}$ [Cm^{-2}]	-	17.91

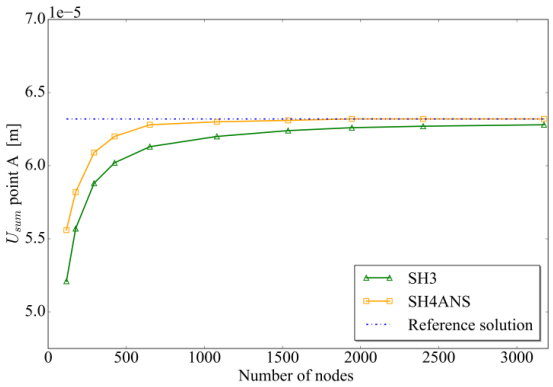

Fig. 14 Active funnel - convergence of the FE results

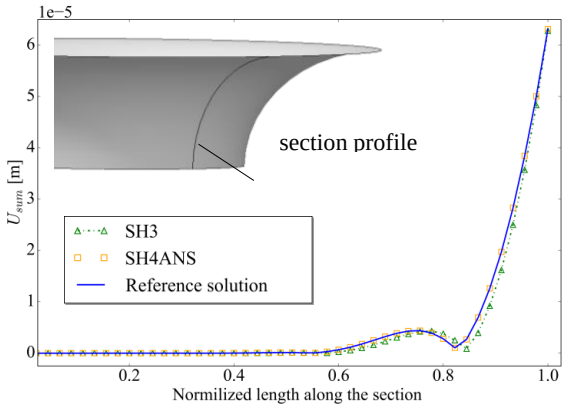

Fig. 15 Active funnel – displacement magnitude along the section profile

The results are given in Fig. 14. As a reference solution, the converged FE solution reported by Nestorovic *et al.* (2014), who used a full biquadratic piezoelectric 9-node shell element, is used.

Furthermore, using the FE meshes that yield converged solution, the displacement magnitude along the section profile is computed and compared to the results by Nestorovic *et al.* (2014). The results presented in Fig. 15 show a good agreement.

6. Conclusions

The integration of multifunctional material based elements into passive structures enabled design solutions capable of sensing and actively responding to external stimuli. This paper focuses on the thin-walled structures with piezoelectric patches as actuators and sensors, which is a distinctive, rather diverse and growing group of adaptive structures.

Two linear shell elements are proposed for modeling and simulation of their behavior, which involves the electro-mechanical coupled field effects. The obvious advantage is high numerical efficiency, but it comes inevitably at the price of rather stiff element elastic behavior. Two known distinctive techniques were applied to address the issues known as locking effects. The co-rotational approach was applied to extend the applicability of the elements to geometrically nonlinear analysis in an efficient manner. Besides the consideration of the element rigid-body rotation, the stress stiffening effects are also included in the formulation. The applied co-rotational approach is suitable for deformations characterized by finite local rotations but small strains and is therefore applicable to the considered type of structures.

The verification of the shell elements was done by a set of examples that cover linear and geometrically nonlinear, static and dynamic analyses, in which both the actuator and sensor functions of piezolayers were addressed. The convergence rate of the elements was shown to be good in the considered examples, which is attributed to the applied techniques as a remedy for the locking effects. The examples have also demonstrated the significance of accounting for the geometrically nonlinear effects, even if, at the first glance, they may appear negligible.

Finally, the current adaptive structures can be seen as a mere skeleton of what is expected in near future. Numerical tools are supposed to speed up the development and improve various design aspects.

References

Aladwani, A., Aldraihem, O. and Baz, A. (2014), "A distributed parameter cantilevered piezoelectric energy harvester with a dynamic magnifier", *Mech. Adv. Mater. Struct.*, **21**(7), 566-578.

Aridogan, U. and Basdogan, I. (2015), "A review of active vibration and noise suppression of plate-like structures with piezoelectric transducers", *J. Intel. Mat. Syst. Str.*, **26**(12), 1455-1476.

Berthelot, J.M. (1999), *Composite materials: mechanical behavior and structural analysis*, Springer-Verlag, New York, US.

Biswal, A.R., Roy, T. and Behera, R.K. (2017), "Optimal vibration energy harvesting from nonprismatic piezolaminated beam", *Smart Syst. Struct.*, **19**(4), 403-413.

Bletzinger, K.U., Bischoff, M. and Ramm, E. (2000), "A unified approach for shear-locking-free triangular and rectangular shell finite elements", *Comput. Struct.*, **75**(3), 321-334.

Braess, D. and Kaltenbacher, M. (2008), "Efficient 3D – finite element formulation for thin mechanical and piezoelectric structures", *Int. J. Numer. Meth. Eng.*, **73**(2), 147-161.

Carrera, E. (2003), "Theories and finite elements for multilayered plates and shells: A unified compact formulation with numerical assessment and benchmarking", *Arch. Comput. Meth. Engng*, **10**, 215-296.

Carrera, E. and Valvano, S. (2017), "Analysis of laminated composite structures with embedded piezoelectric sheets by variable kinematic shell elements", *J. Intel. Mat. Syst. Str.*, DOI: https://doi.org/10.1177/ 1045389X17704913

Cinefra, M., Carrera, E. and Valvano, S. (2015a), "Variable Kinematic shell elements for the analysis of electro-mechanical problems", *Mech. Adv. Mater. Struct.*, **22**(1-2), 77-106.

Cinefra, M., Valvano, S. and Carrera, E. (2015b), "A layer-wise MITC9 finite element for the free-vibration analysis of plates with piezo-patches", *Int. J. Smart Nano Mater.*, **6**(2), 84-104.

Crisfield M.A. (1991), *Non-Linear Finite Element Analysis of Solids and Structures, Volume 1: Essentials*, John Wiley & Sons, Chichester, England.

Felippa, C. and Haugen, B. (2005), "A unified formulation of small-strain corotational finite elements: I. theory", *Comput.*

Meth. Appl. Mech. Eng., **194**, 2285–2335.
Gabbert, U., Duvigneau, F. and Ringwelski, S. (2017), "Noise control of vehicle drive systems", *Facta Universitatis Series Mechanical Engineering*, **15**(2), 183-200.
Gabbert, U., Köppe, H., Seeger, F. and Berger, H. (2002), "Modeling of smart composite shell structures", *J. Theor. Appl. Mech.*, **3**(40), 575-593.
Gabbert, U. and Tzou, H.S. (Eds.) (2000), *Smart Structures And Structronic Systems*, Kluwer Academic Publishers, Amsterdam, Holand
Gupta, V.K., Seshu, P. and Kurien Isaac, K. (2004), "Finite element and experimental investigation of piezoelectric actuated smart shells", *AIAA J.*, **42**(10), 2112-2123.
Huynh, T.C. and Kim, J.T. (2017), "Quantitative damage identification in tendon anchorage via PZT interface-based impedance monitoring technique", *Smart Syst. Struct.*, **20**(2), 181-195.
Lee, S., Cho, B.C., Park, H.C., Goo, N.S. and Yoon K.J. (2004) "Piezoelectric actuator-sensor analysis using a three-dimensional assumed strain solid element", *J. Intel. Mat. Syst. Str.*, **15**(5), 329-338.
Lentzen, S., Klosowski, P. and Schmidt, R. (2007), "Geometrically nonlinear finite element simulation of smart piezolaminated plates and shells", *Smart Mater. Struct.*, **16**, 2265-2274.
Li, F.M., Yao, G. and Zhang, Y. (2016), "Active control of nonlinear forced vibration in a flexible beam using piezoelectric material", *Mech. Adv. Mater. Struct.*, **23**(3), 311-317.
Liu, G.R., Dai, K.Y. and Lim, K.M. (2004), "Static and vibration control of composite laminates integrated with piezoelectric sensors and actuators using the radial point interpolation method", *Smart Mater. Struct.*, **13**, 1438-1447.
Marinkovic, D. and Marinkovic, Z. (2012), "On FEM modeling of piezoelectric actuators and sensors for thin-walled structures", *Smart Struct. Syst.*, **9**(5), 411-426.
Marinkovic, D. and Rama, G. (2017), "Co-rotational shell element for numerical analysis of laminated piezoelectric composite structures", *Composites Part B: Eng.*, **125**, 144-156.
Marinković, D., Köppe H. and Gabbert, U. (2006), "Numerically efficient finite element formulation for modeling active composite laminates", *Mech. Adv. Mater. Struct.*, **13**(5), 379-392.
Marinkovic, D., Köppe, H. and Gabbert, U. (2008) "Degenerated shell element for geometrically nonlinear analysis of thin-walled piezoelectric active structures", *Smart Mater. Struct.*, **17**(1), 1-10.
Marinković, D., Köppe, H. and Gabbert, U. (2009), "Aspects of modeling piezoelectric active thin-walled structures", *J. Intel. Mat. Syst. Str.*, **20**(15), 1835-1844.
Marinkovic, D., Zehn, M. and Marinkovic, Z. (2012), "Finite element formulations for effective computations of geometrically nonlinear deformations", *Adv. Eng. Softw.*, **50**, 3-11.
Masmoudi, S., Mahi, A.E. and Turki, S. (2015), "Use of piezoelectric as acoustic emission sensor for in situ monitoring of composite structures", *Composites Part B: Eng.*, **80**, 307-320.
Militello, C and Felippa C.A. (1990), "A variational justification of the assumed natural strain formulation of finite elements", *NASA Contractor Report 189063.*
Nestorovic, T., Shabadi, S., Marinkovic, D. and Trajkov, M. (2013), "Modeling of piezoelectric smart structures by implementation of a user defined shell finite element", *Facta Universitatis Series Mechanical Engineering*, **11**(1), 1-12.
Nestorovic, T., Shabadi, S., Marinkovic, D. and Trajkov, M. (2014), "User defined finite element for modeling and analysis of active piezoelectric shell structures", *Meccanica*, **49**(8), 1763-1774.
Nguyen-Thoi, T., Phung-Van, P., Thai-Hoang, C. and Nguyen-Xuan, H. (2013), "A Cell-based Smoothed Discrete Shear Gap method (CS-DSG3) using triangular elements for static and free vibration analyses of shell structures", *Int. J. Mech. Sci.*, **74**, 32-45.
Nguyen, V.A., Zehn, M. and Marinković, D. (2016), "An efficient co-rotational FEM formulation using a projector matrix", *Facta Universitatis Series Mechanical Engineering*, **14**(2), 227-240.
Oveisi, A. and Nestorovic, T. (2016), "Mu-synthesis based active robust vibration control of an MRI inlet", *Facta Universitatis Series Mechanical Engineering*, **14**(1), 37-53.
Piefort, V. (2001), "Finite element modeling of piezoelectric active structures", Ph.D. Dissertation, Université Libre de Bruxelle.
Rabinovitch, O. (2005), "Geometrically nonlinear behavior of piezoelectric laminated plates", *Smart Mater. Struct.*, **14**(4), 785-798.
Rama, G. (2017), "A 3-Node piezoelectric shell element for linear and geometrically nonlinear dynamic analysis of smart structures", *Facta Universitatis Series Mechanical Engineering*, **15**(1), 31-44.
Simoes Moita, J.M., Mota Soares, C.M. and Mota Soares, C.A. (2002), "Geometrically non-linear analysis of composite structures with integrated piezoelectric sensors and actuators", *Compos. Struct.*, **57**, 253-261.
To, C.W.S. and Liu, E. (2003), "Analysis of Laminated composite shell structures with piezoelectric components", *Mech. Electromagnetic Solids*, **3**, 229-250.
Valvano, S. and Carrera, E. (2017), "Multilayered plate elements with node-dependent kinematics for the analysis of composite and sandwich structures", *Facta Universitatis Series Mechanical Engineering*, **15**(1), 1-30.
Vertuccio, L., Guadagno, L., Spinelli, G., Lamberti, P., Tucci, V. and Russo, S. (2016), "Piezoresistive properties of resin reinforced with carbon nanotubes for health-monitoring of aircraft primary structures", *Composites Part B: Eng.*, **107**, 192-202.
Willberg, C. and Gabbert, U. (2012), "Development of a three-dimensional piezoelectric isogeometric finite element for smart structure applications", *Acta Mech*, **223**, 1837-1850.
Zemčík, R., Rolfes, R., Rose, M. and Tessmer, J. (2007), "High performance four node shell element with piezoelectric coupling for the analysis of smart laminated structures", *Int. J. Numer. Meth. Eng.*, **70**(8), 934-961.
Zhang, L.W., Song, Z.G. and Liew, K.M. (2016) "Optimal shape control of CNT reinforced functionally graded composite plates using piezoelectric patches", *Composites Part B: Eng.*, **85**, 140-149.
Zhang, S.Q., Chen, M., Zhao, G.Z., Wang, Z.X., Schmidt, R. and Qin X.S. (2017), "Modeling techniques for active shape and vibration control of macro-fiber composite laminated structures", *Smart Syst. Struct.*, **19**(6), 633-641.
Zhang, S. (2014), "Nonlinear FE simulation and active vibration control of piezoelectric laminated thin-walled smart structures", Ph.D. Dissertation, Institute of General Mechanics RWTH Aachen University.

CC